Video Article

Scalable Stamp Printing and Fabrication of Hemiwicking Surfaces

Thomas Germain[1], Chance Brewer[1], James Scott[1], Shawn A. Putnam[1]

[1]Department of Mechanical and Aerospace Engineering, University of Central Florida

Correspondence to: Shawn A. Putnam at Shawn.Putnam@ucf.edu

URL: https://www.jove.com/video/58546
DOI: doi:10.3791/58546

Keywords: Engineering, Issue 142, engineering, stamping, hemiwicking, microfluidics, thin-film deposition, experimental fluid dynamics

Date Published: 12/18/2018

Citation: Germain, T., Brewer, C., Scott, J., Putnam, S.A. Scalable Stamp Printing and Fabrication of Hemiwicking Surfaces. *J. Vis. Exp.* (142), e58546, doi:10.3791/58546 (2018).

Abstract

Hemiwicking is a process where a fluid wets a patterned surface beyond its normal wetting length due to a combination of capillary action and imbibition. This wetting phenomenon is important in many technical fields ranging from physiology to aerospace engineering. Currently, several different techniques exist for fabricating hemiwicking structures. These conventional methods, however, are often time consuming and are difficult to scale-up for large areas or are difficult to customize for specific, nonhomogeneous patterning geometries. The presented protocol provides researchers with a simple, scalable, and cost-effective method for fabricating micro-patterned hemiwicking surfaces. The method fabricates wicking structures through the use of stamp printing, polydimethylsiloxane (PDMS) molding, and thin-film surface coatings. The protocol is demonstrated for hemiwicking with ethanol on PDMS micropillar arrays coated with a 70 nm thick aluminum thin-film.

Video Link

The video component of this article can be found at https://www.jove.com/video/58546/

Introduction

Recently there has been increased interest in being able to both actively and passively control the wetting, evaporation, and mixing of fluids. Uniquely textured hemiwicking surfaces provide a novel solution for cooling techniques because these textured surfaces act as a fluid (and/or heat) pump without the moving parts. This fluid motion is driven by a cascade of capillary action events associated with the dynamic curvature of the liquid thin-film. In general, when a fluid wets a solid surface, a curved liquid thin-film (*i.e.,* liquid meniscus) rapidly forms. The fluid thickness and curvature profile evolve until a free-energy minimum is reached. For reference, this dynamic wetting profile can rapidly decay to tens of nanometers in thickness within a spanning (fluid-wetting) length-scale of only tens of micrometers. Thus, this transitional (liquid-film) region can undergo significant changes in liquid-interface curvature. The transitional (thin-film) region is where nearly all the dynamic physics and chemistry originates. In particular, the transitional (thin-film) region is where maximum (1) evaporation rates, (2) dis-joining pressure gradients, and (3) hydrostatic pressure gradients are found[1,2]. As a result, curved liquid-films play a vital role in thermal transport, phase separation, fluid instabilities, and the mixing of multi-component fluids. For instance, with respect to heat transfer, the highest wall heat fluxes have been observed in this highly curved, transitional thin-film region[3,4,5,6,7].

Recent hemiwicking studies have shown that the geometry (*e.g.,* height, diameter, *etc.*) and placement of the pillars determine the wetting front profile and velocity of the fluid running through the structures[8]. As the fluid front is evaporating off the end of the last structure in an array, the fluid front is maintained at a constant distance and curvature, as the evaporated fluid is being replaced by the fluid stored in the wicking structures[9]. Hemiwicking structures have also been used in heat pipes and on boiling surfaces to analyze and enhance different heat transfer mechanisms.[10,11,12].

One method currently used to create wicking structures is thermal imprint lithography[13]. This method is performed by stamping the desired layout into a resist layer on a silicon mold sample with a thermoplastic polymer stamp, then removing the stamp to maintain the microstructures. Once removed, the sample is put through a reactive ion etching process to remove any of the excess resist layer[14,15]. This process, however, can be sensitive to the temperature of the fabrication of the wicking structures and includes multiple steps that utilize various coatings to ensure the accuracy of the wicking structures[16]. It is also the case that lithography techniques are not practical for macro-scale patterning; while they still provide a way to create a pattern of microstructures on a surface, the throughput of this procedure is far less than ideal for large-scale reproduction. Considering large-scale, reproducible texturing, such as spin or dip coating, there is an inherent lack of controllable patterning. These methods create a random array of microstructures on the target surface but can be scaled to cover vastly larger areas than traditional lithography techniques[17].

The protocol outlined within this report attempts to combine the strengths of traditional texturing methods while simultaneously eliminating the specific weaknesses of each; it defines a way to fabricate custom hemiwicking structures of various heights, shapes, orientations, and materials on a macro-scale and with potentially high throughput. Various wicking patterns can be quickly created for the purpose of optimization of wicking characteristics, such as directional control of fluid velocity, propagation, and mixing of different fluids. The use of different wicking structures can

also provide varying thin-film thickness and curvature profiles, which can be used to systematically study the coupling between heat and mass transfer with different thickness and curvature profiles of the liquid meniscus.

Protocol

1. Create the Patterning Map

1. Using a graphics editor, create the desired pattern for the hemiwicking structures represented as a bitmap image.
   NOTE: Some of the wicking design parameters (*i.e.,* angle gradient, depth gradient) can be made to be dependent on the grayscale values assigned to each pixel. These grayscale values are then edited in order to modify the desired parameter.
2. Save the bitmap as a portable network graphic (.png) and place the file in a readily available folder.

2. Placing the Plastic to be Stamped for Molding

1. Begin by translating the stamping bit away from the workspace to avoid any accidental contact that may cause breakage of the tip (+*z* displacement, **Figure 1**).
2. Secure the plastic stamping mold/wafer to a backing plate for subsequent stamping on the *x*, *y* translation stage (see **Figure 1**). Secure the sample/backing plate on to the x, y motorized stamping stage (**Figure 1**)
3. Align the center of the plastic mold/wafer with the stamping axis of the stamping bit. This is accomplished *via* computerized ±*x* and ±*y* displacements with the *x, y* motorized stamping stage.
4. Translate the stamping bit towards the plastic mold/wafer (-*z* displacement, **Figure 1**) until the stamping bit is almost in contact with the mold/wafer surface.

3. Stamping the Plastic Sample for PDMS Molding

1. Using the computerized stamping control program, set the distance between the stamping bit (tip) and the plastic mold/wafer surface.
2. Translate the stamping bit in small increments (-δ*z* displacement, **Figure 1**) towards the surface of the sample until the tooling is in contact with the plastic.
   NOTE: The bit should only **lightly contact** the surface.
3. After contact, translate the stamping bit away from the sample to avoid any possible contact between the bit and sample during subsequent translation (δz ≈ 100 μm).
4. Assign a pixel distance (in micron), maximum and minimum cavity depth (in micron), maximum and minimum angle (in degrees), initial *x* and *y* pixel position of the pattern, and pixel threshold for any gray-scale linked patterning for the stamping procedure.
5. Upload the patterning map (created in step 1.1) to be read by the program. Based on the pixel distance and the patterning map, the locations of all the stamps are sent to the stepper motors.
6. Ensure that the heating laser is focused on the tip of the stamping bit and only activates while the stamping bit is moving toward and into the plastic mold.
7. Create the cavities by pressing the bit into the plastic while following the patterning map to achieve the desired hemiwicking pattern.
8. Remove the stamped plastic mold for subsequent surface refinishing and polishing.
9. Polish the surface of the plastic mold using 9000 grit, finer wet/dry sandpaper.
   NOTE: Alternatively, micro-mesh abrasive can be used to ensure the removal of surface deposits that cause cratering around the pillars in the PDMS mold.

4. Create the PDMS Molding

1. Pour 2 g of elastomer base and 0.2 g of the elastomer curing agent into a beaker and mix together thoroughly for 3 min.
2. Place the mixture into an evacuated chamber to release any air bubbles caught in the mixture; this step may need to be repeated multiple times.
   NOTE: For samples of varying volume requirements, adjust the amount of base and curing agent as needed while maintaining a 10:1 ratio.
3. Place the stamped plastic mold into a walled container, ideally not much larger than the outer diameter of the mold, for the curing to occur.
4. Pour the PDMS mixture free of air pockets onto the stamped plastic and within the container. Pour in a spiral, starting from the center of the stamped area, to attempt to distribute the PDMS mixture as equally as possible.
5. Repeat step 4.2 for any air pockets that may have formed from pouring the mixture onto the stamped pattern. Place the PDMS mixture and plastic piece with stamped pattern onto a hot plate and heat the assembly at 100 °C for 15 min. Then heat an additional 25 min at 65 °C.
6. Allow the PDMS mixture to cool and cure for 20 min before handling.
7. Cut the edges of the PDMS plastic away from the container wall and remove the PDMS plastic from the mold. Store the PDMS plastic in a covered container to avoid dust particles from collecting on the surface.

5. Depositing the Thin-Film Metal on the PDMS

1. Place the sample PDMS inside the deposition chamber leaving enough space for the shutter to be opened and closed unobstructed.
2. Depressurize the deposition chamber to at least 10 mTorr.
3. Engage the dry pump system and set the spin rate to 75 kRPM. Allow chamber to reach a pressure on the order of 10^{-8} Torr.
   NOTE: This will remove most contaminants from the chamber; process may take up to 12 h to complete.
4. Power on the cooler and DC power supply and set the power to 55 W.

5. Open the argon valve slightly and pressurize the chamber to the order of 10^{-3} Torr. Set the dry pump system 50 kRPM and wait until this set speed is achieved.
6. Reduce power to 35 W and depressurize the chamber to 13 mTorr. Open the shutter to ignited plasma and start the timer.
   NOTE: Ignited plasma should give off a blue, incandescent glow. Timer should be set for desired thickness of film deposit. It has been determined that for 35 W and pressure of approximately 13 mTorr, a rate of 7 nm deposition per minute is expected.
7. Once the desired film thickness has been achieved, close the shutter and turn off power supply.
8. Close all of the valves within the deposition chamber and turn off the dry pump system. Allow time for the dry-pump fan to come to a complete stop.
9. Slowly pressurize the chamber until it reaches local atmospheric pressure and remove the sample, storing it for future experiments.

Representative Results

Figure 1 provides a schematic of how the stamping mechanism would create the mold for the wicking structures on a plastic mold. To investigate the quality of the stamping apparatus in manufacturing wicking films, two different pillar arrays were created to analyze the quality of the pillars for future wicking experiments. Aspects of the apparatus investigated were the accuracy of the height of the pillars (with and without a depth gradient), the quality of the pillars after the PDMS molding, the quality of the pillars after the sputter deposition process, and the ability of the structures to create hemi-wicking. To accomplish this, two wicking pattern variants were created, one that displayed a depth gradient and another of uniform depth.

Figure 2a shows the bitmap that was used in order to create the depth and angle gradients. It can be seen that every pillar column was assigned a different gray scale value varying from 0 to 95. This was done in order to have a different depth for each pillar column. **Figures 2b** and **2c** display the pillars on the PDMS created by the molding process. This verifies that the gray scale values were used impact the depth in the plastic molding and therefore the height of the pillar on the PDMS sample. Table 1 outlines the data from the depth gradient and shows the percentage of the expected height from the stamping pattern. These data were gathered from measurements on 50 pillars, or one complete array, displayed in **Figure 2**. The expected height of the pillar with the given gray scale values were calculated from the following equation:

$$h_{exp} = h_{max} - (h_{max} - h_{min})\left(\frac{GSV}{PT}\right) \quad (1)$$

where h_{exp} is the expected height, h_{max} is the maximum height as defined by the user, h_{min} is the minimum height as defined by the user, PT is the pixel threshold as defined by the user and GSV is the gray scale value. It can be seen that for a gray scale value of zero (*i.e.,* black), the expected height will be the maximum height and while the gray scale value is equal to the pixel threshold, the expected height will be the minimum height.

Figure 3a shows the bitmap file used to create a larger wicking structure array of constant pillar height. Every black pixel represents a cavity location, with the distance between stamping instances defined in the program through the pixel distance. This binary approach, in contrast with **Figure 1a**, creates a uniform array of angle and pillar heights. **Figure 3b** and **3c** provide a top and side view of the pillars, respectively. It can be seen that despite a uniform-height pillar specification, the process produced undersize pillars. While the maximum height was set to 100 µm, it was found that the average height of the pillars was roughly 71.89 ± 10.18 µm, based on 38 pillars. This can be attributed to possible imperfections that can be found in the cavities while they are being made or due to possible air pockets that had formed and remained in the holes.

Figure 4 displays four individual images of the pillars after aluminum was deposited on the PDMS sample. **Figure 4a** and **4b** show the side and top view of the pillars, respectively, without a working fluid in the wicking structure. Similar to what was seen with the PDMS sample, the heights of the samples were not consistent across all of the pillars. The heights and standard deviations of the PDMS and Al samples are compared and displayed in **Table 2**. These data were gathered after measuring pillars (n = 38) both before and after the deposition of aluminum on the PDMS. Notable surface roughness was also present; it is thought that the sanding procedure used on the sample plate transferred to the PDMS sample and was mirrored onto the surface of the aluminum film. It is also possible that the roughness is solely attributed to the deposition process.

Figure 4c and **4d** visualize the side and top views of the pillars, respectively, with a working fluid in the wicking structure. The working fluid that was used in this example was ethanol. However, water does not exhibit the same hemi-wicking occurrence as ethanol does with this sample. This phenomenon can be attributed to the following (or combination of): 1) a non-ideal surface texture, 2) residual surface roughness (as shown in **Figure 4b**), 3) impurities in the aluminum coating, and 4) too thin of a native aluminum oxide layer. With that said, ethanol was able to wick because the lyophilicity of the aluminum oxide that formed on the aluminum surface. Even though aluminum dioxide is lyophilic, it does not show hydrophilic characteristics, prohibiting the water from wicking. The use of chemical surface treatments to the PDMS wicking structure is another method that can be used to alter the hydrophilicity of the sample -*e.g.*, wet chemistry processing can be used to create hydrophylic self-assembling monolayers (SAMs)[18]. Despite these imperfections, this proves that the wicking structure created through the described procedure is able to create hemi-wicking for a working fluid.

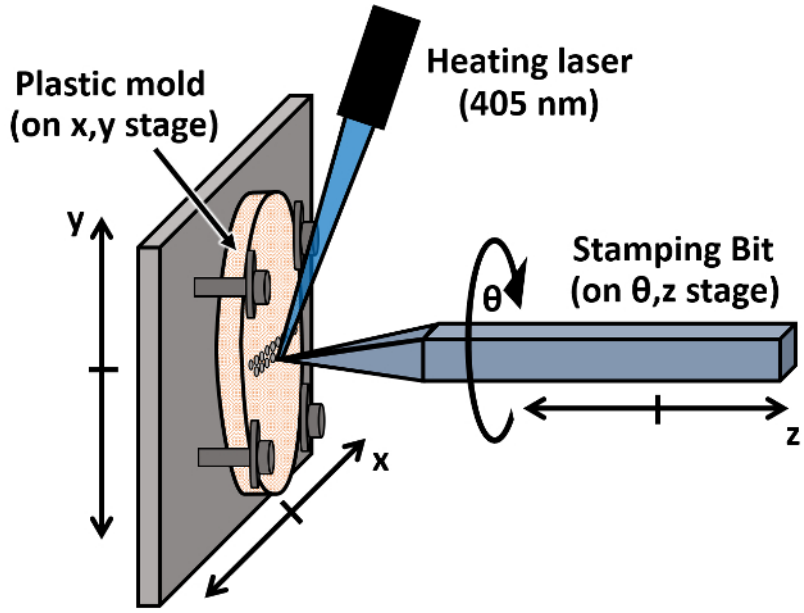

Figure 1: The schematic of the stamping bit apparatus for fabrication of micro-patterned plastic molds. The movement of the plastic mold along the *x*- and *y*- axes is determined by two computer-controlled stepper motor/stages (one for each direction). Likewise, the stamping angle (*θ*) and stamping depth (Δ*z*) of the stamping bit are controlled by two separate, computer-controlled stepper motor/stages. The computer-controlled heating laser is activated while the bit is creating the stamping cavity in the plastic mold. Please click here to view a larger version of this figure.

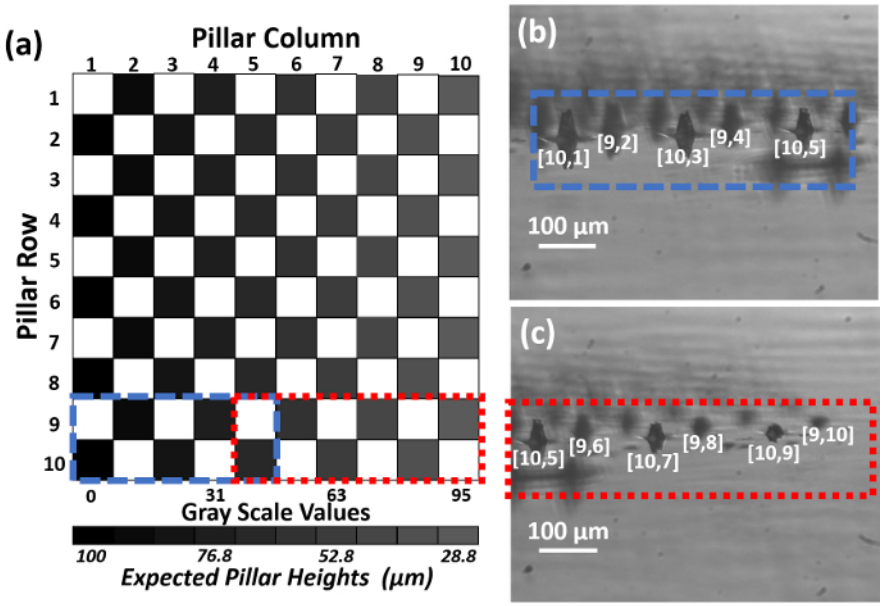

Figure 2: The depth-gradient pillar array pattern and PDMS base. (a) The bitmap used for fabricating a 'depth-gradient' micropillar array. For imprinting, the pixel threshold is set to 100, the maximum depth is set to 100 μm, the minimum depth is set to 25 μm, and each pixel is set to represent a distance of 100 μm. Based on these values, each row is separated by 100 μm while the distance between two pillars within a row is 200 μm. The gray scale value of each pixel determines the distance the stamping bit travels into the plastic mold. Therefore, as the gray scale values increase going across the bitmap, the heights of the pillars decrease. The expected heights of the pillars with the corresponding gray scale values are provided. **(b)** Images of pillar columns 1 through 5 for the PDMS base from the blue box area at the bottom left hand corner of the Bitmap. **(c)** Images of pillar columns 5 through 10 for the PDMS base from the red box at the bottom right hand corner of the bitmap. The image pixel distance for **(b)** and **(c)** is 0.335 μm/pixel. Please click here to view a larger version of this figure.

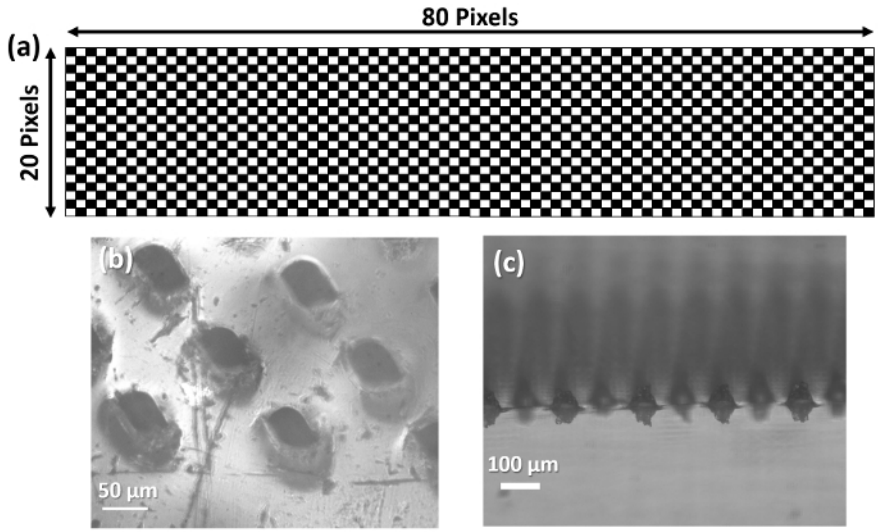

Figure 3: The pattern and PDMS base for the wicking structures for hemiwicking. (a) The bitmap used to create the rectangular wicking structure. The depth is set to 100 µm and each pixel is set to represent a distance of 100 µm. Since all the gray scale values are the same in this bitmap, all of the pillar heights should be the same. Also, similar to the pattern in **Figure 2**, each row is separated by 100 µm while the distance between two pillars within a row is 200 µm. **(b)** A top view of the pillars of the PDMS wicking structure that is casted using the plastic mold based on the bitmap in **(a)**. The image resolution is 0.176 µm/pixel. **(c)** A side view of the pillars of the PDMS wicking structure that is casted using the plastic mold based on the bitmap in **(a)**. Unlike the wicking structures presented in **Figure 2**, the pillar heights in the wicking structure are more consistent in height. The image resolution is 0.723 µm/pixel. Please click here to view a larger version of this figure.

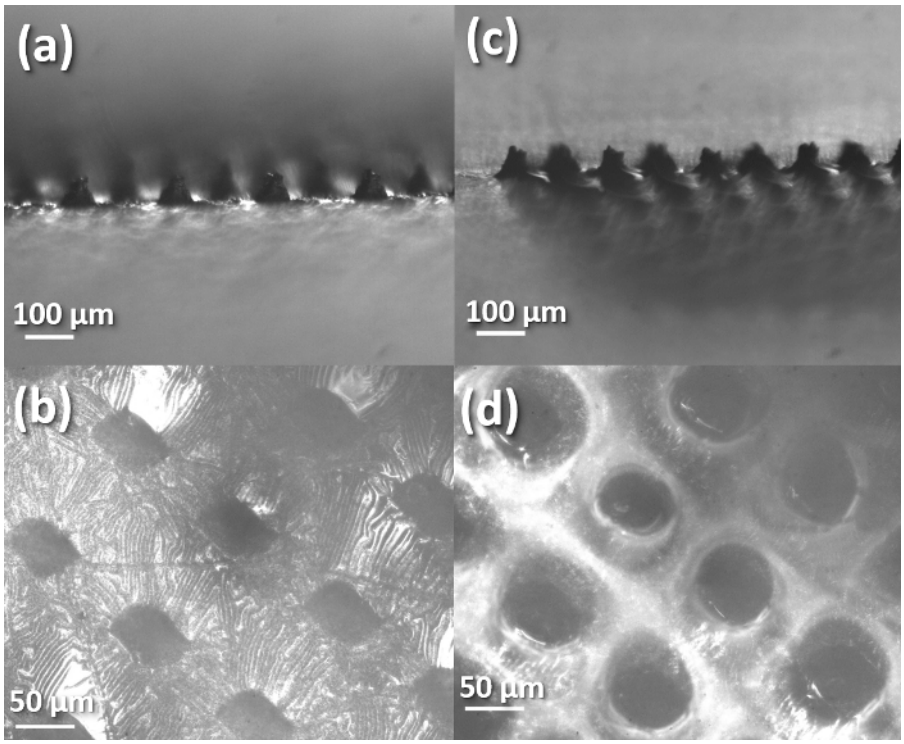

Figure 4: The wicking structures after Al deposition with and without hemiwicking. (a) A side view of the wicking pillars created in **Figure 3** after the Al deposition without ethanol. The thickness of the aluminum on top of the PDMS is roughly 70 µm. **(b)** A top view of the wicking pillars created in **Figure 3** after the Al deposition without ethanol. **(c)** A side view of the wicking pillars created in **Figure 3** after the Al deposition with ethanol wicking in the structures (the ethanol can mostly be seen along the base of the focused pillars). **(d)** A top view of the wicking pillars created in **Figure 3** after the Al deposition with ethanol wicking in the structures. For **(a)** and **(c)**, the image resolution is 0.723 µm/pixel and for **(b)** and **(d)**, the image resolution is 0.176 µm/pixel. Please click here to view a larger version of this figure.

Pillar	Gray Scale Value	Expected Height (μm)	Measured Height (μm)	% of Expected
1	0	100	59.6	59.6
			± 4.58	
2	10	92.5	59.71	64.55
			± 5.88	
3	21	84.25	54.71	64.94
			± 5.57	
4	31	76.75	46.48	60.56
			± 2.61	
5	42	68.5	46.59	68.01
			± 5.21	
6	53	60.25	38.92	64.6
			± 1.62	
7	63	52.75	31.8	60.28
			± 0.73	
8	74	44.5	26.58	59.73
			± 1.49	
9	85	36.25	20.13	55.53
			± 1.44	
10	95	28.75	16.01	55.69
			± 1.94	

Table 1: The expected and measured heights of all the pillar columns for the depth gradient pattern.

	Expected Height (μm)	Mean Measured Height (μm)	Standard Deviation (μm)
PDMS Sample Without Al Deposit	100	71.89	10.18
PDMS Sample With Al Deposit	100	61.59	8.493

Table 2: PDMS with and without Al deposition pillar height comparison.

Discussion

A method has been introduced to create patterned pillar arrays for hemiwicking structures; this is accomplished by imprinting cavities on a plastic wafer with an engraving apparatus that follows patterning from a bitmap created by the user. A PDMS mixture is then poured, cured and coated with a thin film of aluminum *via* deposition. The pillar array characteristics can be customized depending on the gray scale value that is assigned in the bitmap following this protocol. This crucial aspect of patterning can create a wide range of possible wicking structures to test that can be used in various applications, including thin-film research and direct applications in thermal systems. Another area of variety not mentioned in **Representative Results** is the angle gradient that can be implemented in the array. Similar to the depth gradient, changing the gray scale value of different pixels can change the angle of the drill bit (θ, **Figure 1**).

Another major step that should be taken note of is the creation of the PDMS base. Differences in the pillar heights and the deformities on and around the pillars are common in the wicking structures. Abrading the surface with micro-mesh or abrasive slurries helps create symmetric samples and even PDMS thickness. In addition, the evacuation and heat treatment processes were designed to take place simultaneously, as heating elements were incorporated within the mold itself. This effectively limits handling by the user and any associated irregularities, as well as airborne contamination (*i.e.,* dust particulate) during the curing phase. These considerations will be implemented for future samples.

The deposition of material onto the PDMS base is another important step that must be tailored to each experiment. The conditions mentioned in the protocol are aluminum specific and as such, must change as the depositing material changes. If another metal is preferred, changes in power output, chamber pressure, and sputtering time should be altered in order to obtain the ideal surface conditions for the desired depositing material. For future samples, metals with different surface energies (*i.e.*, gold, germanium) will be deposited to test their respective wicking capabilities. When depositing the different metals in the future, the protocol must be updated in order to properly deposit the desired metal onto the PDMS.

The biggest problem that has been introduced in the procedure of making the hemiwicking structures is the surface roughness of the sample. It can be seen that surface defects exist on the PDMS mold (**Figure 3b**) and on the Al surface (**Figure 3b, 3d**); this could stem from either the sanding process or the metal deposition process. The surface defects are viewed as problematic, as surface defects can affect the wicking

speed and front distance of the working fluid. An ideal experiment would have a smooth surface on and between the pillars, so the fluid is able to flow through the wicking structure unhindered by the surface conditions. The proposed solution is to use higher grade (*i.e.,* finer grit) abrasives for sanding the plastic wafer prior to deposition, as well as longer sanding times. As seen from **Table 1** and **Table 2**, the pillar heights are not manufactured as expected based on the values given to the stepper motors. This could be due to deflection of the sample along the stamping axis while the bit is imprinting into the plastic. This issue can be resolved by increasing the distance the bit has to travel into the plastic; this, however, leaves a possible inconsistency with the pillar heights and pillar-base diameters for future experiments. Methods must be developed in order to limit the amount of deflection the sample experiences, such as increasing the temperature of the tip to limit the resistance from the plastic, or securing the sample in a different way.

While challenges remain in refining the stamping process, the outlined method is effective for creating ordered arrays of comparable geometry. The methodology used to create hemiwicking structures, or any micro-patterned surface feature, shows that samples can be rapidly produced for later processing at other labs or research companies at a low cost and at a faster rate than contemporary methods. These hemiwicking structures can be easily fabricated to replicate the optimal thin-film curvature and wicking front velocity. The wicking front velocity would be measured using a high-speed camera analyzing the fluid front traveling from pillar to pillar. Simultaneously, the thickness and curvature profile can be obtained using a reflectometry and interferometry approach that has been proven in previous experiments on the edge pillars[6]. The self-regulating nature of the wicking structures will help maintain a constant thin-film region for analysis, despite the different surface energies in varying fluids and on the surface. With this method, wicking structure variants can be fabricated quickly for the purposes of understanding the effects wicking geometry has on the thin-film region and wicking front of different fluids.

Disclosures

The authors have no disclosures to mention for this paper.

Acknowledgements

This material is based on research partially sponsored by the United States Office of Naval Research under Grant No. N00014-15-1-2481 and the National Science Foundation under Grant No. 1653396. The views and conclusions contained herein are those of the authors and should not be interpreted as necessarily representing the official policies or endorsements, either expressed or implied, of U.S. Office of Naval Research, the National Science Foundation, or the United States Government.

References

1. Plawsky, J. L., *et al.* Nano- and Micro-structures for Thin Film Evaporation - A Review. *Nanoscale and Microscale Thermophysical Engineering.* **18**, 251-269 (2014).
2. Derjaguin, B. V., Churaev, N. V., On the question of determining the concept of disjoining pressure and its role in the equilibrium and flow of thin films. *Journal of Colloid and Interface Science.* **66**, 389 (1978).
3. Ma, H. B., Cheng, P., Borgmeyer, B., Wang, Y. X. Fluid flow and heat transfer in the evaporating thin film region. *Microfluidics and Nanofluidics.* **4** (3), 237-243 (2008).
4. Hohmann, C., Stephan, P. Microscale temperature measurement at an evaporating liquid meniscus. *Experimental Thermal and Fluid Science.* **26** (2-4), 157-162 (2002).
5. Potask Jr., M., Wayner Jr., P.C. Evaporation from a two-dimensional extended meniscus. *International Journal of Heat Mass Transfer.* **15** (10), 1851-1863 (1972).
6. Panchamgam, S. S., Plawsky, J. L., Wayner, P. C. Microscale heat transfer in an evaporating moving extended meniscus. *Experimental Thermal and Fluid Science.* **30** (8), 745-754 (2006).
7. Arends, A. A., Germain, T. M., Owens, J. F., Putnam, S. A. Simultaneous Reflectometry and Interferometry for Measuring Thin-film Thickness and Curvature. *Review of Scientific Instruments.* **89** (5) (2018).
8. Zhu, Y., Antao, D. S., Lu, Z., Somasundaram, S., Zhang, T., Wang, E.N. Prediction and characterization of dry out heat flux in micropillar wick structures. *Langmuir.* **32** (7) 1920-1927 (2016).
9. Kim, J., Moon, M. W., Kim, H. Y. Dynamics of hemiwicking. *Journal of Fluid Mechanics.* **800**, 57-71 (2016).
10. Ding, C., Soni, G., Bozorgi, P., Meinhart, C. D., MacDonald, N. C. Wicking Study of Nanostructured Titania Surfaces for Flat Heat Pipes. *Nanotech Conference & Expo, Houston, TX.* (2009).
11. Chen, R., Lu, M. C., Srinivasan, V., Wang, Z., Cho, H. H., Majumdar, A. Nanowires for Enhanced Boiling Heat Transfer. *Nano Letters.* **9** (2), 548-553 (2009).
12. Kim, B. S., Choi, G., Shim, D. II, Kim, K. M., Cho, H. H. Surface roughening for hemi-wicking and its impact on convective boiling heat transfer. *International Journal of Heat and Mass Transfer.* **102**, 1100-1107 (2016).
13. Mikkelsen, M. B. *et al.* Controlled deposition of sol-gel sensor material using hemiwicking. *Journal of Micromechanics and Microengineering.* **21** (11) (2011).
14. Haatainen, T., Ahopelto, J. Pattern Transfer using Step&Stamp Imprint Lithography. *Physica Scripta.* **67** (4), 357-360 (2003).
15. Chou, S.Y., Krauss, P. R., Renstrom, P. J. Nanoimprint lithography. *Journal of vacuum Science & Technology B: Microelectronics and Nanometer Structures Processing, Measurement, and Phenomena.* **14** (6), 4129 (1996).
16. Pozzato, A. *et al.* Superhydrophobic surfaces fabricated by nanoprint lithography. *Microelectronic Engineering.* **83** (4-9), 884-888 (2006).
17. Nair, R. P., Zou, M. Surface-nano-texturing by aluminum-induced crystallization of amorphous silicon. *Surface and Coatings Technology.* **203** (5-7), 675-679 (2008).
18. Ashby, P. D., Lieber, C. M. Ultra-sensitive Imaging and Interfacial Analysis of Patterned Hydrophilic SAM Surfaces Using Energy Dissipation Chemical Force Microscopy. *Journal of the American Chemical Society.* **127** (18), 6814-6818 (2005).

